International Journal of Heat and Mass Transfer 56 (2013) 340–349

Contents lists available at SciVerse ScienceDirect

International Journal of Heat and Mass Transfer

journal homepage: www.elsevier.com/locate/ijhmt

Analysis of the multidimensional effects in biofilms

Michael Hauser, Kambiz Vafai *

Department of Mechanical Engineering, University of California, Riverside, CA, United States

ARTICLE INFO

Article history:
Received 15 July 2012
Received in revised form 17 September 2012
Accepted 17 September 2012

Keywords:
Biofilm
Continuum mechanics
Mathematical model
Multidimensional
Error maps

ABSTRACT

A general multidimensional, multispecies, heterogenous biofilm model is developed using the balance equations. Multidimensional effects are studied by taking limiting scenarios towards lower dimensional analogs, as well as studying the effects of changing biofilm surface geometries. Error maps are developed suggesting when single-dimensional models give an accurate representation of biofilm growth, and when multidimensional effects are substantial. A porous media model is studied, where the bacteria *Pseudomonas aeruginosa* is modeled to grow in a packed porous bed of spheres. It is found that under most circumstances, single-dimensional models predict very similar growth rates as compared to their multidimensional analogs. However, under some conditions the multidimensionality can have a significant effect in the model's predictions. To the authors' best knowledge, this is the first work which develops error maps detailing multidimensional effects of biofilm growth.

1. Introduction

Biofilms are communities of bacterial cells that are adherent to surfaces and are protected by a self-created extracellular polymeric substance. Free floating, planktonic bacteria can exhibit very different traits when compared to the same species of bacteria inhabiting a biofilm. In order for a biofilm to develop, a bacterial cell must adhere to a surface. From this point, other planktonic cells may attach to this initial cell, or instead they may also attach to the substratum. The attached bacteria then grow and divide, increasing the communal population of the biofilm. Through the use of quorum sensing, the bacteria can communicate their population and coordinate activation of various traits.

It is common for different species of bacteria to live together and compete for nutrients and space, thus multispecies and multisubstrate effects are important attributes to include in the development of comprehensive biofilm models. There exists a diverse set of methods used to model these interactions, with the most popular being to model the biofilm using continuum mechanics [1–5], individual-based models [6–8], cellular automaton [9,10], and combinations there-of [11,12].

Earlier work in biofilm modeling led to fairly simple yet powerful one dimensional continuum models, with one dimensional growth occurring orthogonal to the substratum [1,13,14]. One dimensional continuum models can have the ability to capture important effects, such as species competition for space and nutrients, which leads to a globally heterogenous biofilm structure [1]. Biofilm heterogeneity is a result of different species having different nutrient uptake rates, different growth rates and different EPS production rates. Heterogeneity in nutrient concentration is also captured in these one dimensional models, in part since different nutrients have different diffusion rates as well as different consumption rates. These are very important effects, which can be captured in one dimension.

Drawbacks to one dimensional models are that, for some cases which constitute a smaller subset of available scenarios, spatial heterogeneities do not necessarily occur only in the direction orthogonal to the substratum, but instead growth and diffusion processes can also occur parallel to that plane. If a spatial gradient exists in the nutrient concentration in the horizontal direction, then one would have a horizontal component of the nutrient flux. This would also result in bacterial species growing along this gradient, leading to a heterogeneous distribution of bacterial species in the horizontal direction within the biofilm. The impact of these types of growths needs to be assessed.

For example, in nutrient limited regimes and under conditions with sufficiently large mass transfer boundary layers biofilm fingering formation can occur [2,3], which is a multidimensional effect. This complex surface geometry affects nutrient diffusion processes, which itself affects species growth rates. By using one-dimensional models one is ignoring the effects of the surface geometry.

A second example of a multidimensional system is seen in a partially mixed multispecies system. One would expect to see spatial heterogeneities of bacterial species in the vertical as well as

* Corresponding author.
E-mail address: vafai@engr.ucr.edu (K. Vafai).

0017-9310/$ - see front matter © 2012 Elsevier Ltd. All rights reserved.
http://dx.doi.org/10.1016/j.ijheatmasstransfer.2012.09.034

Nomenclature

Dependent variables

$\rho_s = \rho_s(x, y, z, t)$ density of species s
$v_s = v_s(x, y, z, t)$ volume fraction of species s
$C_n = C_n(x, y, z, t)$ concentration of nutrient n
$\vec{S} = \vec{u}(x, y, Z(x, y, t))$ parametric form of surface
$\vec{u} = \vec{u}(x, y, z, t)$ biofilm expansion velocity
$\Phi = \Phi(x, y, z, t)$ biofilm expansion potential

Reaction rates

$g_s = g_s(x, y, z, t)$ growth rate for species s
$r_n = r_n(x, y, z, t)$ reaction rate for nutrient n

Scaling factors

L_x domain width in x-direction
L_y domain width in y-direction
$Z = Z(x, y, t)$ functional form of surface
τ characteristic time scale

Constants

ρ_s^* density of species s
D_n constant scalar diffusion coefficient for nutrient n
λ biomass detachment coefficient
μ_s growth rate of species s
K_n^s monod saturation constant for species s and nutrient n
b_s endogenous rate constant for species s
k_s inactivation rate constant for species s
Y_s biomass yield for species s
α_s conversion factor for species s
$C_{n\mathrm{B}}$ bulk fluid concentration for nutrient n
i stoichiometric factor – EPS/*Pa*
k stoichiometric factor – Gl/O_2

Dimensionless variables

x' dimensionless x-variable
y' dimensionless y-variable
z' dimensionless z-variable
t' dimensionless time-variable

horizontal directions, and considering different bacterial species have different growth and consumption properties, these heterogeneities can lead to multidimensional species competition [2,6].

It is the purpose of this work to study and assess these multidimensional characteristics, their absolute influences on net growth rate, and finally to develop error maps which can be used to suggest when multidimensional characteristics are necessary for accurate prediction of biofilm growth.

2. Governing equations

The derivations of the governing equations have been influenced by previous work [1,2,4,5]. The biofilm is assumed to live in three spatial dimensions and one temporal dimension, i.e. $\mathbb{R}^3 \otimes \mathbb{R}$.

The biofilm is assumed to have continuous properties and growth will follow the continuity equation. Since biofilm expansion is convection dominated, for bacterial species s:

$$\frac{\partial \rho_s}{\partial t} + \vec{\nabla} \cdot (\vec{u}\, \rho_s) = g_s \tag{1}$$

The dependent variables are defined such that ρ_s is the density of species s, g_s is the growth rate of species s, and $\vec{u}$ is the biofilm expansion velocity. If it is assumed that the density of species s across the biofilm domain is constant $\rho_s^* \in \mathbb{R}$, then $\rho_s = \rho_s^* v_s$, where v_s is the volume fraction of species s in the biofilm. The biofilm growth equation becomes:

$$\frac{\partial v_s}{\partial t} + \vec{\nabla} \cdot (\vec{u}\, v_s) = \frac{g_s}{\rho_s^*} \tag{2}$$

Using the fact that $\sum_s v_s = 1$, one finds:

$$\vec{\nabla} \cdot \vec{u} = \sum_s \frac{g_s}{\rho_s^*}. \tag{3}$$

The growth equations can then be simplified to:

$$\frac{\partial v_s}{\partial t} + \vec{u} \cdot \vec{\nabla} v_s = \frac{g_s}{\rho_s^*} - v_s \sum_i \frac{g_i}{\rho_i^*} \tag{4}$$

Nutrient concentration for nutrient n within the biofilm is diffusion dominated and can be presented as:

$$\frac{\partial C_n}{\partial t} = D_n \nabla^2 C_n + r_n \tag{5}$$

The dependent variables are defined such that C_n is the nutrient concentration for nutrient n and r_n is the reaction rate. Since diffusion processes occur much faster than biofilm growth processes, and we are interested in biofilm growth processes, one may assume that the nutrient concentration has reached steady state over biofilm growth process time scales [15].

$$D_n \nabla^2 C_n + r_n = 0 \tag{6}$$

An order of magnitude argument can be made to justify this approximation. Diffusion coefficients of nutrients within biofilm are of order $D \sim 100 \times 10^{-6}$ m^2/days while lengths scales of biofilm are of order $l \sim 10^{-3}$ m, which imply that nutrient diffusion velocities within biofilm are of order $v_D \sim D/l \sim 10^{-1}$ m/days. Furthermore, biofilm grow to length scales of order $l \sim 10^{-3}$ m in $t \sim 10$ days, which implies that biofilm growth velocities are of order $v_G \sim l/t \sim 10^{-4}$ m/days. Thus diffusion velocities are 3 orders of magnitude greater than growth velocities, implying that the steady state approximation of nutrient diffusion is valid.

The parametric form of the biofilm surface $\vec{S}(x, y, t) = (x, y, Z(x, y, t))$ is related to the expansion velocity as follows:

$$\frac{\partial \vec{S}}{\partial t} = \vec{u}\,|_{z=Z} \tag{7}$$

The integral form of this differential equation is:

$$\vec{S} = \vec{S_o} + \int_0^t \vec{u}\, dt \tag{8}$$

One way in which shearing forces can be incorporated into the model is by modifying the differential equation for the biofilm surface [1]:

$$\frac{\partial \vec{S}}{\partial t} = \vec{u}\,|_{z=Z} - \lambda Z^2 \hat{z} \tag{9}$$

where λ is a constant specifying the relative strength of shearing forces.

The governing equations can be simplified by assuming irrotational growth [2,3]. The expansion velocity may then be taken as the negative gradient of a scalar potential $\vec{u} = -\vec{\nabla}\mathbf{\Phi}$. The governing equations in the final, coordinate-free form can be presented as:

$$\frac{\partial v_s}{\partial t} - \vec{\nabla}\mathbf{\Phi} \cdot \vec{\nabla} v_s = \frac{g_s}{\rho_s^*} - v_s \sum_i \frac{g_i}{\rho_i^*} \tag{10}$$

$$D_n\nabla^2 C_n + r_n = 0 \tag{11}$$

$$\nabla^2\mathbf{\Phi} = -\sum_i \frac{g_i}{r_i^*} \tag{12}$$

$$\vec{S} = \vec{S}_o - \int_0^t \vec{\nabla}\mathbf{\Phi}\mathrm{d}t \tag{13}$$

For all of the equations, the boundary conditions are assumed to be periodic in the horizontal directions and no-flux at the substratum. For the nutrient equations, a constant bulk fluid nutrient concentration is taken at the surface of the biofilm. For the potential equation, because of the gauge freedom associated with defining a potential, we define the potential at the biofilm surface to be zero.

3. Analysis and solution methodology

One of the major difficulties associated with multidimensional biofilm modeling is tracking the moving boundary and defining a boundary condition on this dynamically changing boundary. The method used here is to solve the sets of equations in a specifically chosen curvilinear coordinate space, chosen such that the generally varying biofilm surface boundary will be constant in the new coordinate space. Thus some of the difficulties associated with defining a boundary condition on the oddly shaped, dynamically moving biofilm surface will not be problematic. A second method often employed for tracking the moving boundary is by solving the equations within a level-set framework [2,3,16].

A significant advantage to defining the boundary conditions in this new coordinate space is that one is able to study biofilm growth over large changes in length scales. This is clearly appropriate to biofilm modeling because biofilm start as individual bacteria, which have length scales on the order of micrometers, and they can grow to become entire biofilm communities, which have length scales on the order of millimeters, which is a change of three orders of magnitude. A disadvantage of using this solution method is that since one is working in a curvilinear coordinate system, three-dimensional simulations can take much longer to finish. After the calculations are done in the curvilinear space, one must then convert back to Euclidean space to make physical sense of the results. The derivation of the coordinate transformation is presented in three spatial dimensions, however the two dimensional derivation is completely analogous.

If L_x and L_y are the widths of the domain, $Z(x,\ y,\ t)$ the biofilm surface, and τ the characteristic time scale, then define the coordinate mapping as follows:

$$x' = \frac{x}{L_x} \tag{14}$$

$$y' = \frac{y}{L_y} \tag{15}$$

$$z' = \frac{z}{Z(x,\ y,\ t)} \tag{16}$$

$$t' = \frac{t}{\tau} \tag{17}$$

Finding the new derivative operators requires knowledge of the Jacobian matrix $\frac{\partial}{\partial x^a} = J_a^b \frac{\partial}{\partial x'^b}, a, b = 1,\ 2,\ 3,\ 4$. Einstein summation notation is used, where a repeated index implies summation and $\frac{\partial}{\partial x^a} = \partial_a$ is written for brevity. The new derivative operators are:

$$\frac{\partial}{\partial x} = \frac{1}{L_x}\frac{\partial}{\partial x'} - \frac{z'}{L_x}\frac{\partial_{x'}Z}{Z}\frac{\partial}{\partial z'} \tag{18}$$

$$\frac{\partial}{\partial y} = \frac{1}{L_y}\frac{\partial}{\partial y'} - \frac{z'}{L_y}\frac{\partial_{y'}Z}{Z}\frac{\partial}{\partial z'} \tag{19}$$

$$\frac{\partial}{\partial z} = \frac{1}{Z}\frac{\partial}{\partial z'} \tag{20}$$

$$\frac{\partial}{\partial t} = \frac{1}{\tau}\frac{\partial}{\partial t'} - \frac{z'}{\tau}\frac{\partial_{t'}Z}{Z}\frac{\partial}{\partial z'} \tag{21}$$

In the new coordinate space, the Laplacian operator expands to the following:

$$\begin{aligned}\nabla^2 = {} & \frac{1}{L_x^2}\frac{\partial^2}{\partial x'^2} + \frac{1}{L_y^2}\frac{\partial^2}{\partial y'^2} + \frac{1}{Z^2}\left(1 + z'\left(\left(\frac{\partial_{x'}Z}{L_x}\right)^2 + \left(\frac{\partial_{y'}Z}{L_y}\right)^2\right)\right)\frac{\partial^2}{\partial z'^2} \\ & - 2\frac{z'}{L_x^2}\frac{\partial_{x'}Z}{Z}\frac{\partial^2}{\partial x'\partial z'} - 2\frac{z'}{L_y^2}\frac{\partial_{y'}Z}{Z}\frac{\partial^2}{\partial y'\partial z'} \\ & + \frac{z'}{Z^2}\left(\frac{2(\partial_{x'}Z)^2 - (\partial_{x'}^2 Z)Z}{L_x^2} + \frac{2(\partial_{y'}Z)^2 - (\partial_{y'}^2 Z)Z}{L_y^2}\right)\frac{\partial}{\partial z'}\end{aligned} \tag{22}$$

With the derivative operators defining the new vector space, the initial and boundary conditions may be set. For brevity the boundary conditions are defined in terms of the Euclidean derivative operators instead of the derivative operators found to describe the new space.

$$\begin{aligned}&\frac{\partial v_s}{\partial t} - \vec{\nabla}\mathbf{\Phi}\cdot\vec{\nabla}v_s = \frac{g_s}{\rho_s^*} - v_s\sum_i \frac{g_i}{\rho_i^*} \\ &\text{I.C.}\quad v_s(x',\ y',\ z',\ 0) = v_{s0}(x',\ y',\ z') \\ &\text{B.C.}\quad v_s(0,\ y',\ z',\ t') = v_s(1,\ y',\ z',\ t'), \\ &v_s(x',\ 0,\ z',\ t') = v_s(x',\ 1,\ z',\ t'),\quad \frac{\partial v_s}{\partial z}(x',\ y',\ 0,\ t) = 0\end{aligned} \tag{23}$$

$$\begin{aligned}&D_n\nabla^2 C_n + r_n = 0 \\ &\text{B.C.}\quad C_n(0,\ y',\ z',\ t') = C_n(1,\ y',\ z',\ t'), \\ &\frac{\partial C_n}{\partial x}(0,\ y',\ z',\ t') = \frac{\partial C_n}{\partial x}(1,\ y',\ z',\ t') \\ &C_n(x',\ 0,\ z',\ t') = C_n(x',\ 1,\ z',\ t'), \\ &\frac{\partial C_n}{\partial y}(x',\ 0,\ z',\ t') = \frac{\partial C_n}{\partial y}(x',\ 1,\ z',\ t') \\ &C_n(x',\ y',\ 1,\ t') = C_{nB}, \frac{\partial C_n}{\partial z}(x',\ y',\ 0,\ t') = 0\end{aligned} \tag{24}$$

$$\begin{aligned}&\nabla^2\mathbf{\Phi} = -\sum_i \frac{g_i}{r_i^*} \\ &\text{B.C.}\quad \mathbf{\Phi}(0,\ y',\ z',\ t') = \mathbf{\Phi}(1,\ y',\ z',\ t'), \\ &\tfrac{\partial\mathbf{\Phi}}{\partial x}(0,\ y',\ z',\ t') = \tfrac{\partial\mathbf{\Phi}}{\partial x}(1,\ y',\ z',\ t') \\ &\mathbf{\Phi}(x',\ 0,\ z',\ t') = \mathbf{\Phi}(x',\ 1,\ z',\ t'), \\ &\tfrac{\partial\mathbf{\Phi}}{\partial y}(x',\ 0,\ z',\ t') = \tfrac{\partial\mathbf{\Phi}}{\partial y}(x',\ 1,\ z',\ t') \\ &\mathbf{\Phi}(x',\ y',\ 1,\ t') = 0,\ \tfrac{\partial\mathbf{\Phi}}{\partial z}(x',\ y',\ 0,\ t') = 0\end{aligned} \tag{25}$$

$$\begin{aligned}&\vec{S} = \vec{S}_o - \textstyle\int_0^t \vec{\nabla}\mathbf{\Phi}\mathrm{d}t \\ &\text{I.C.}\ \vec{S}_0 = (x,\ y,\ Z(x,\ y,\ z,\ 0))\end{aligned} \tag{26}$$

The covariant transformation maps the irregularly shaped biofilm domain onto a square domain in a curvilinear coordinate space. Fourth order accurate finite differencing approximations were applied to these sets of equations on a uniform fixed grid and programmed in *Mathematica*. The first step of the computational scheme was to initialize the surface of the biofilm and volume fractions of the biofilm species. Subsequent steps were to iteratively calculate in time the changing surface, volume fractions, nutrient concentrations and potential. The surface and volume fraction equations were solved explicitly, while the nutrient and potential equations were solved implicitly. Simulations were run on a PC with an Intel Core i7 processor. Two dimensional simulations took up to 5 min to finish, while three dimensional simulations took up to 40 h to finish.

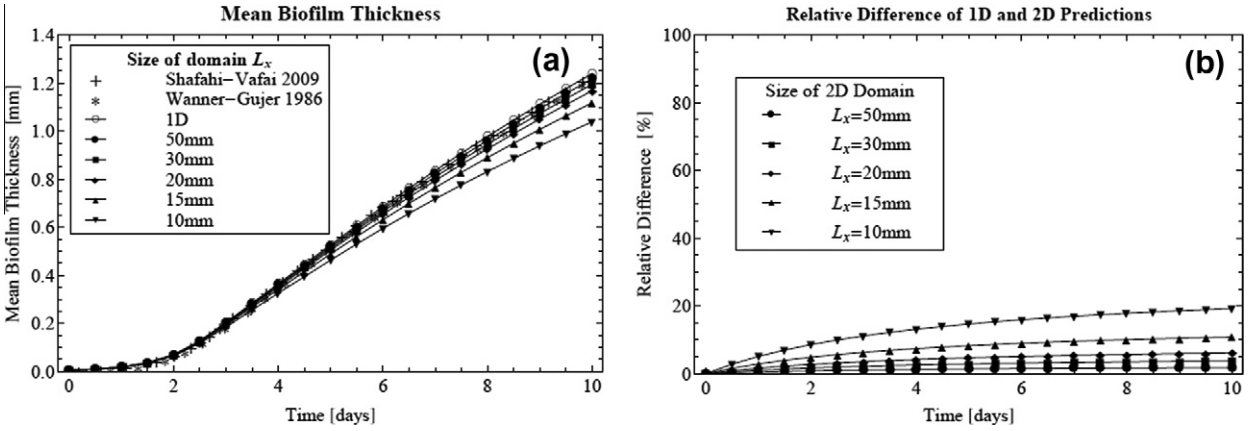

Fig. 1. Comparison between 1D and 2D biofilm growth with variable domain sizes; (a) biofilm growth, (b) relative differences.

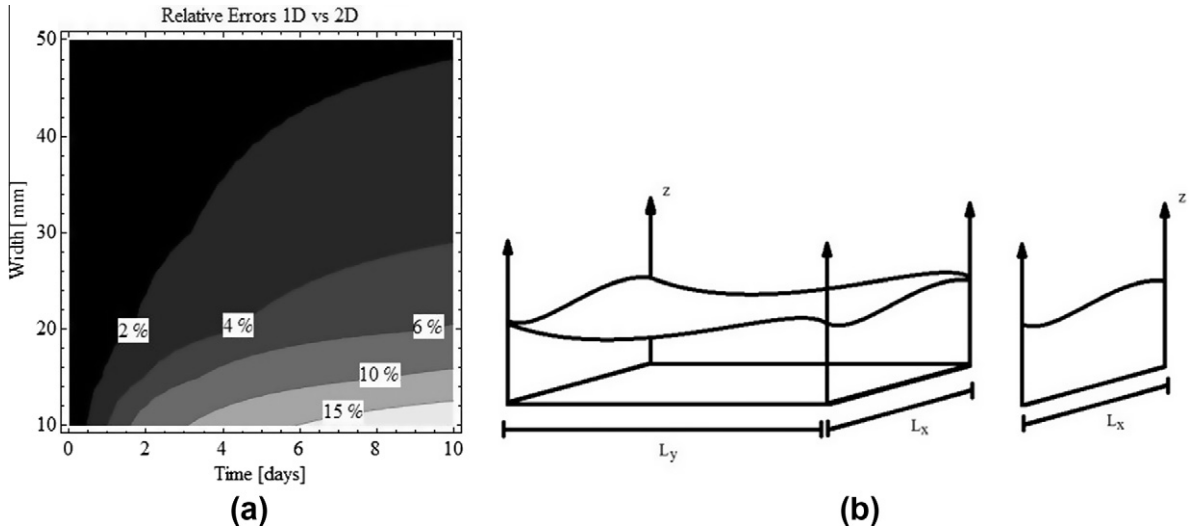

Fig. 2. Biofilm growth over variable domain sizes; (a) interpolation of relative differences between 1D and 2D simulations, (b) illustration of 2D and 3D domain sizes and aspect ratios.

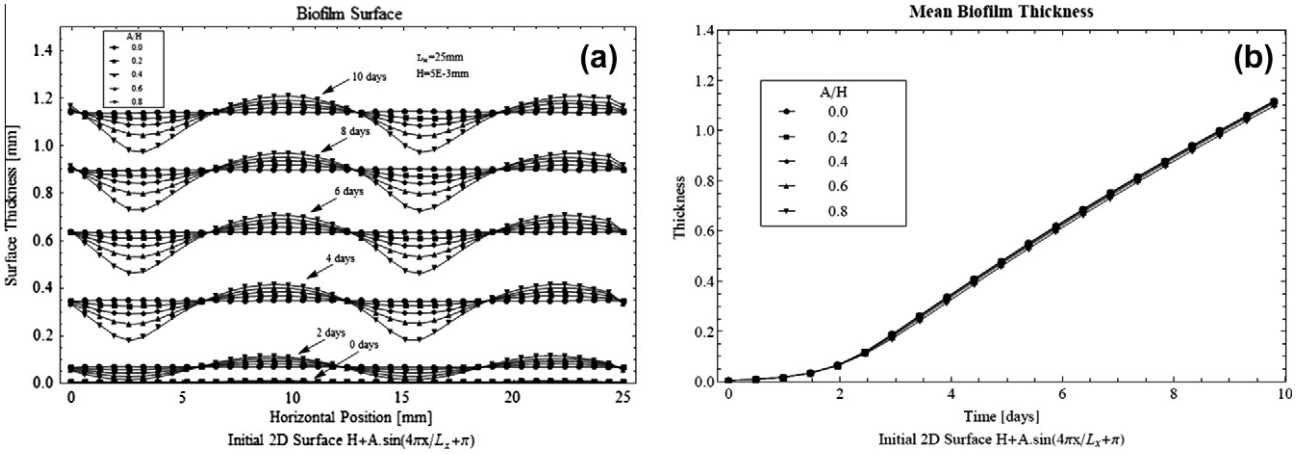

Fig. 3. 2D biofilm growth with variable initial surface perturbation amplitude; (a) visual with surface structure, (b) mean biofilm growth.

4. Biofilm model

4.1. Three species

Solutions were found for a representative biofilm model composed of Heterotrophic bacteria, Autotrophic bacteria and EPS [1,2,4]. Heterotrophic and Autotrophic species consume Glucose and Ammonium, respectively, and they both consume Oxygen. The biofilm growth kinetics are described by monod expressions. For brevity, Heterotrophic, Autotrophic and inert species are denoted by H, A and I, respectively, and Glucose, Ammonium and Oxygen, are denoted by Gl, Am and O_2, respectively. Parameter constants can be found in Wanner–Gujer [1].

$$g_H = \mu_H \rho_H^* v_H \frac{C_{Gl}}{K_{Gl}^H + C_{Gl}} \frac{C_{O_2}}{K_{O_2}^H + C_{O_2}} - b_H \rho_H^* v_H \frac{C_{O_2}}{K_{O_2}^H + C_{O_2}} - k_H \rho_H^* v_H \quad (27)$$

$$g_A = \mu_A \rho_A^* v_A \frac{C_{Am}}{K_{Am}^A + C_{Am}} \frac{C_{O_2}}{K_{O_2}^A + C_{O_2}} - b_A \rho_A^* v_A \frac{C_{O_2}}{K_{O_2}^A + C_{O_2}} - k_A \rho_A^* v_A \quad (28)$$

$$g_I = k_H \rho_H^* v_H + k_A \rho_A^* v_A \quad (29)$$

Nutrient consumption by the biofilm directly affects nutrient concentration within the biofilm:

$$r_{Gl} = -\frac{1}{Y_H} \mu_H \rho_H^* v_H \frac{C_{O_2}}{K_{O_2}^H + C_{O_2}} \frac{C_{Gl}}{K_{Gl}^H + C_{Gl}} \quad (30)$$

$$r_{Am} = -\frac{1}{Y_A} \mu_A \rho_A^* v_A \frac{C_{O_2}}{K_{O_2}^A + C_{O_2}} \frac{C_{Am}}{K_{Am}^A + C_{Am}} \quad (31)$$

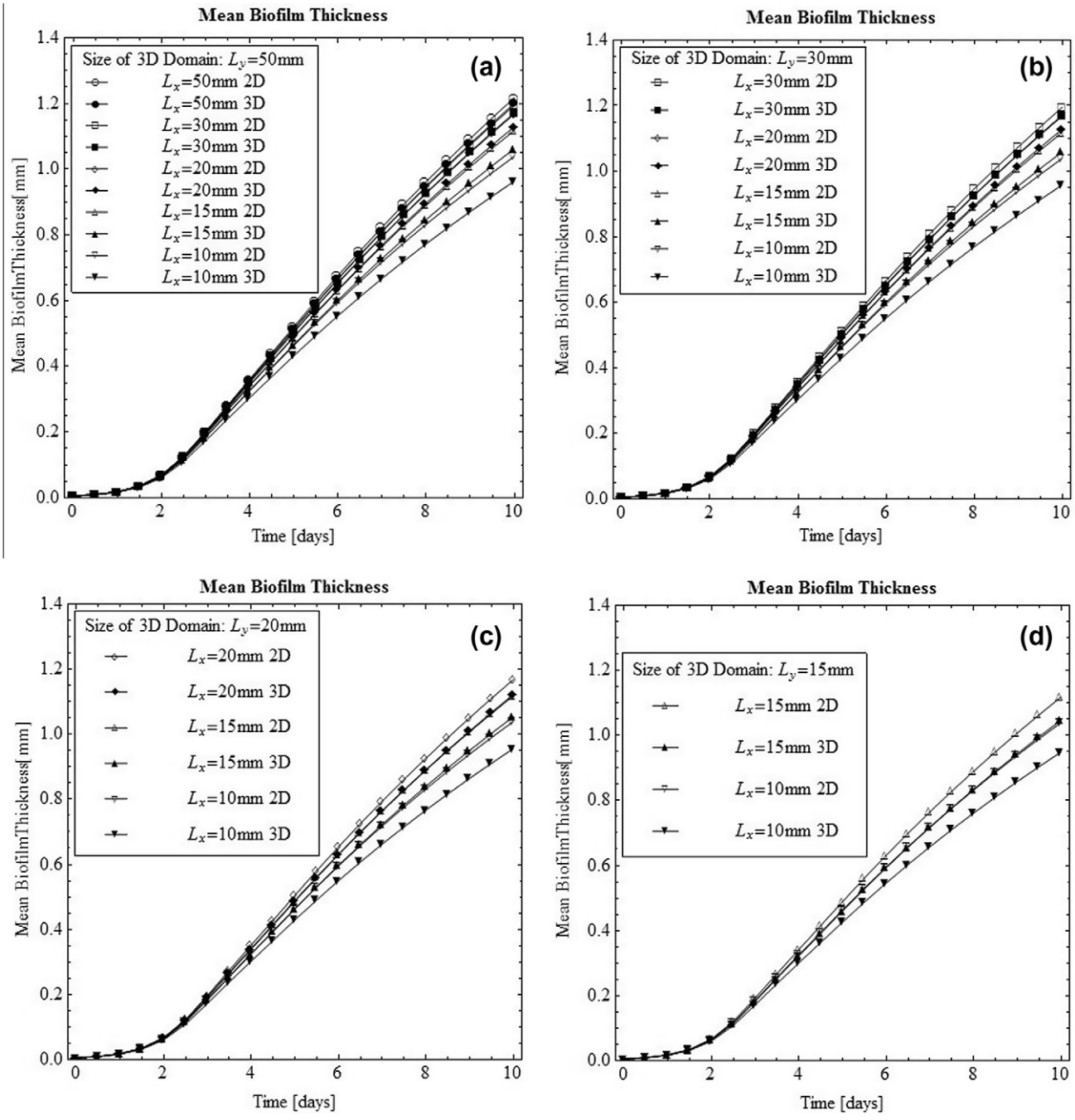

Fig. 4. Comparison between 2D and 3D biofilm growth with variable domain sizes and aspect ratios; (a) L_y = 50 mm, (b) L_y = 30 mm, (c) L_y = 20 mm, (d) L_y = 15 mm.

$$r_{O_2} = -\frac{\alpha_H - Y_H}{Y_H}\mu_H \rho_H^* v_H \frac{C_{O_2}}{K_{O_2}^H + C_{O_2}} \frac{C_{Gl}}{K_{Gl}^H + C_{Gl}} - b_H \rho_H^* v_H \frac{C_{O_2}}{K_{O_2}^H + C_{O_2}} - \frac{\alpha_A - Y_A}{Y_A}\mu_A \rho_A^* v_A \frac{C_{O_2}}{K_{O_2}^A + C_{O_2}} \frac{C_{Am}}{K_{Am}^A + C_{Am}} - b_A \rho_A^* v_A \frac{C_{O_2}}{K_{O_2}^A + C_{O_2}} \quad (32)$$

4.2. Two species

A multidimensional continuum biofilm model is used to study changing permeability of a packed porous bed of spheres. The biofilm is assumed to be composed of the bacterial species *Pseudomonas aeruginosa* and EPS. Growth and diffusion kinetics are described by monod expressions for Glucose and Oxygen, stoichiometric ratios of *Pa* to EPS and Glucose to Oxygen, and yield coefficients. Parameter constants can be found in Wanner–Cunningham–Lundman [17].

$$g_{Pa} = \mu \rho_{Pa}^* v_{Pa} \frac{C_{Gl}}{K_{Gl} + C_{Gl}} \frac{C_{O_2}}{K_{O_2} + C_{O_2}} \quad (33)$$

$$g_{EPS} = k g_{Pa} = k \mu \rho_{Pa}^* v_{Pa} \frac{C_{Gl}}{K_{Gl} + C_{Gl}} \frac{C_{O_2}}{K_{O_2} + C_{O_2}} \quad (34)$$

Nutrient consumption by the biofilm directly effects nutrient concentration within the biofilm:

$$r_{Gl} = -\left(\frac{1}{Y_{Pa/Gl}} + \frac{k}{Y_{EPS/Gl}}\right) g_{Pa} = -\left(\frac{1}{Y_{Pa/Gl}} + \frac{k}{Y_{EPS/Gl}}\right) \mu \rho_{Pa}^* v_{Pa} \frac{C_{Gl}}{K_{Gl} + C_{Gl}} \frac{C_{O_2}}{K_{O_2} + C_{O_2}} \quad (35)$$

$$r_{O_2} = \frac{1}{i} r_{Gl} = -\frac{1}{i}\left(\frac{1}{Y_{Pa/Gl}} + \frac{k}{Y_{EPS/Gl}}\right) \mu \rho_{Pa}^* v_{Pa} \frac{C_{Gl}}{K_{Gl} + C_{Gl}} \frac{C_{O_2}}{K_{O_2} + C_{O_2}} \quad (36)$$

5. Results and discussion

Multidimensional effects are studied by taking limiting scenarios towards lower dimensional analogs. This is done by increasing the size of the domain until it is effectively independent of the dimension. An objective of this work is to establish the limiting conditions which will show when lower dimensional models provide a good approximation to higher dimensional ones. Periodic boundary conditions are used to model part of a large system far from the edges, thus when the size of the computational domain increases, it essentially decreases the resolution of the heterogeneities associated with multidimensional effects. Therefore, if the size of the computational domain increases, then the effects of the multidimensional heterogeneities decreases tending towards a one dimensional model.

5.1. Comparison of one dimensional and two dimensional models

Fig. 1a shows that the one dimensional model predicts higher growth rates than the analogous two dimensional model, and that the two dimensional model converges to the one dimensional model for large domain widths. Also, in Fig. 1a comparisons are shown with the work of Wanner–Gujer [1] and Shafahi–Vafai [4]. As expected, a larger domain yields higher growth rates since in a larger domain the potential would increase more uniformly from

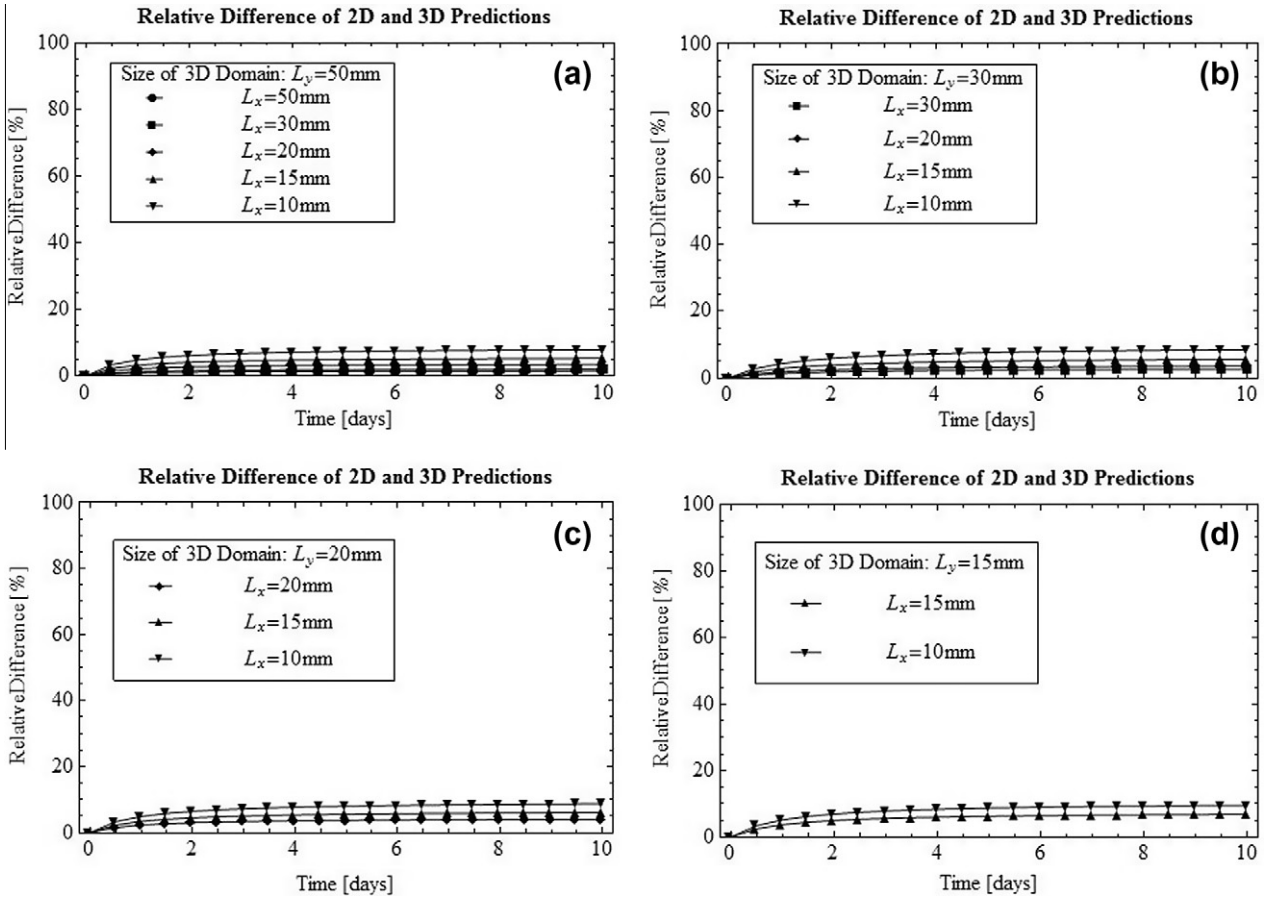

Fig. 5. Relative differences between 2D and 3D Simulations with variable domain sizes and aspect ratios; (a) L_y = 50 mm, (b) L_y = 30 mm, (c) L_y = 20 mm, (d) L_y = 15 mm.

top to bottom. In a smaller domain where multidimensional effects play a more important role, the potential should change relatively more in the horizontal direction, thus horizontal gradients become more relevant. It is expected that parts of these horizontal gradients to interfere with each other, leading to an overall decrease in the biofilm expansion velocity.

As seen in Fig. 1b, the relative difference between the one and two dimensional models increase as the size of the domain decrease. Interpolating over the relative differences gives a continuous error map over variable domain sizes from 10 to 50 mm, as shown in Fig. 2a.

A change in initial surface geometry results in a change in nutrient diffusion behavior within the biofilm domain which results in a change in biofilm growth. Fig. 3a shows the result of changing the relative ratio of surface structure perturbation amplitude to mean initial height. The perturbation is taken to be a sinusoid on the biofilm surface prescribed by where H and A are the initial height and amplitude of the perturbation, respectively.

$$H + A\ \sin(4\pi x/L_x + \pi)$$

Upon averaging the biofilm height over the domain, as seen in Fig. 3b the initial surface geometry plays a minimal role in predicting net biofilm growth, with the net effect averaging out to be similar to a flat surface. The case with a greater varying surface results in slightly slower growth rates, due to the presence of more variations in the horizontal direction at the expense of vertical variations.

5.2. Comparison of two dimensional and three dimensional models

Fig. 2b shows the method used to compare the two dimensional and three dimensional models. Limiting scenarios on the domain were taken such that the domain was shrunk in one direction and held constant in the other, so the shape of the domain is rectangular with a variable aspect ratio. Comparisons were made between the 2D and 3D model predictions. The 2D model effectively matches the 3D model when one domain length is extended beyond a certain limit. Figs. 4 and 5 show the effects of changing the size and aspect ratios of the three dimensional domain, and how the three dimensional models converge to their two dimensional analogs at larger domain sizes.

The domain in Fig. 4a is such that it is held at 50 mm in the y-direction while made smaller in the x-direction. As was shown in the two dimensional case, a 50 mm domain width provides an excellent approximation of the limiting scenario. Thus the three and two dimensional models predict similar values when one domain width direction is held at 50 mm. When the domain is reduced in one direction, due to small widths multidimensional effects become more important in that direction and the two-dimensional model deviates more significantly from the three dimensional growth rate predictions.

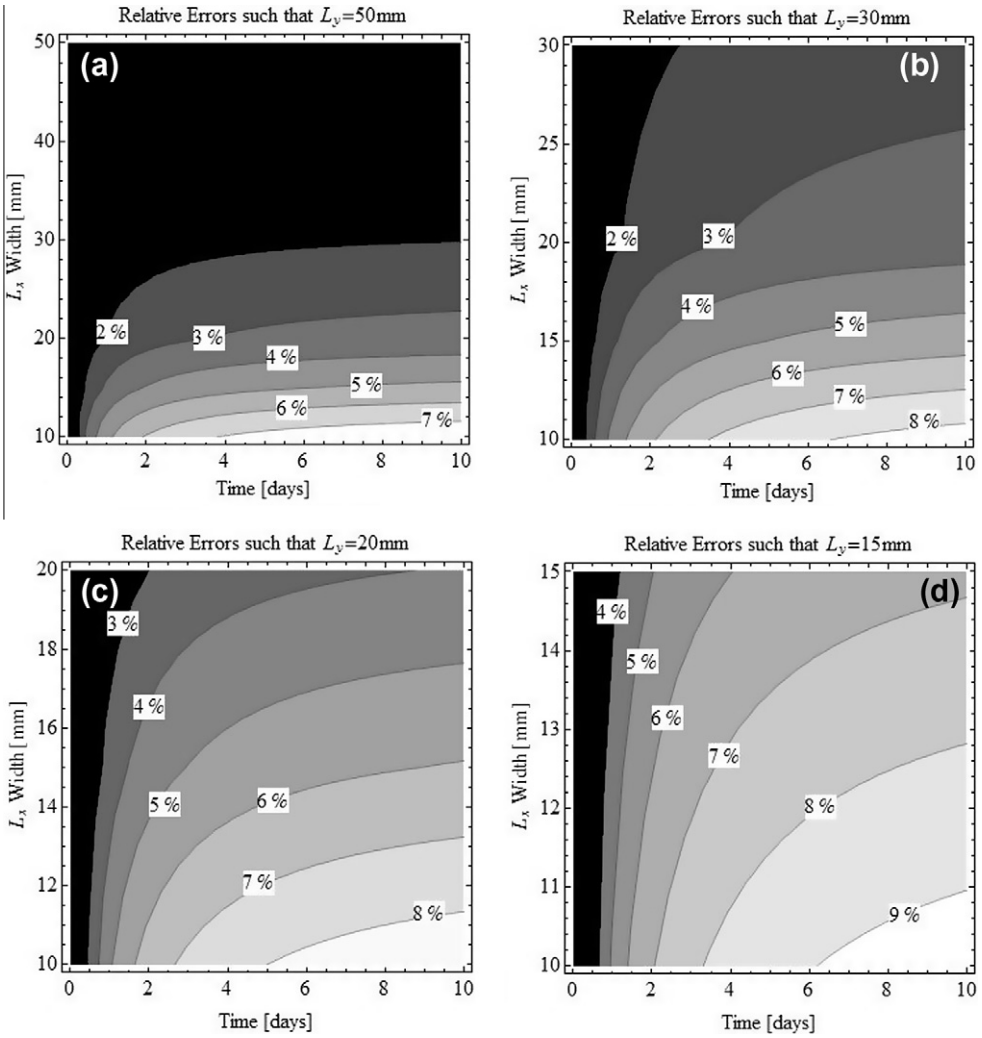

Fig. 6. Interpolation of relative differences between 2D and 3D simulations with variable domain sizes; (a) L_y = 50 mm, (b) L_y = 30 mm, (c) L_y = 20 mm, (d) L_y = 15 mm.

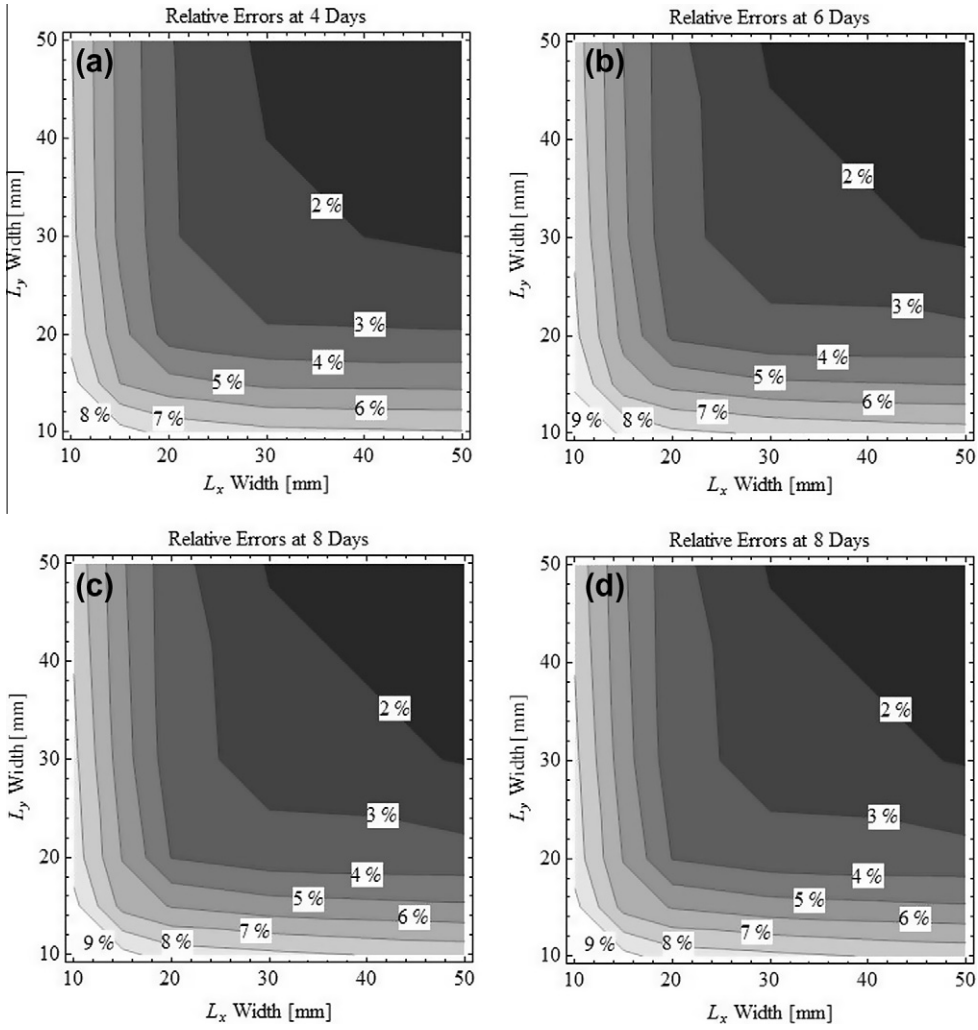

Fig. 7. Spatial error maps displaying the discrepancy in going from 3D to 2D simulations; (a) t = 4 days, (b) t = 6 days, (c) t = 8 days, (d) t = 10 days.

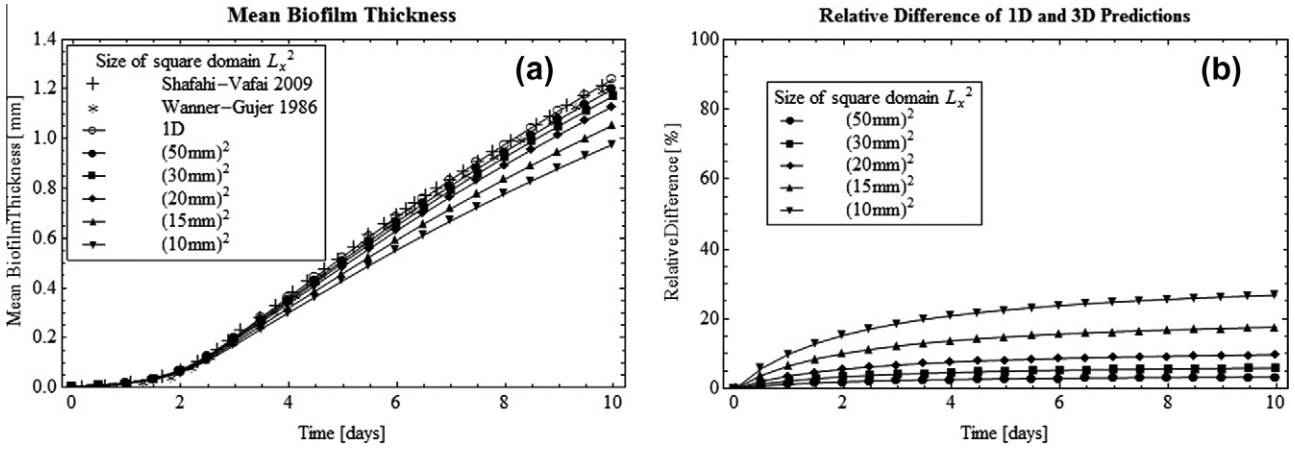

Fig. 8. Comparison between 1D and 3D biofilm growth with variable domain sizes; (a) biofilm growth, (b) relative differences.

As was the case between the 1D and 2D comparisons, the three dimensional biofilm grows more slowly than it does in the equivalent two dimensional case. Again this is because the potential in the three dimensional case varies more in the horizontal directions than in the two dimensional case. Thus the gradient of this potential, which is the biofilm expansion vector, has a larger horizontal component which does not contribute to its vertical growth. Fig. 6 displays the error maps establishing the range of validity of

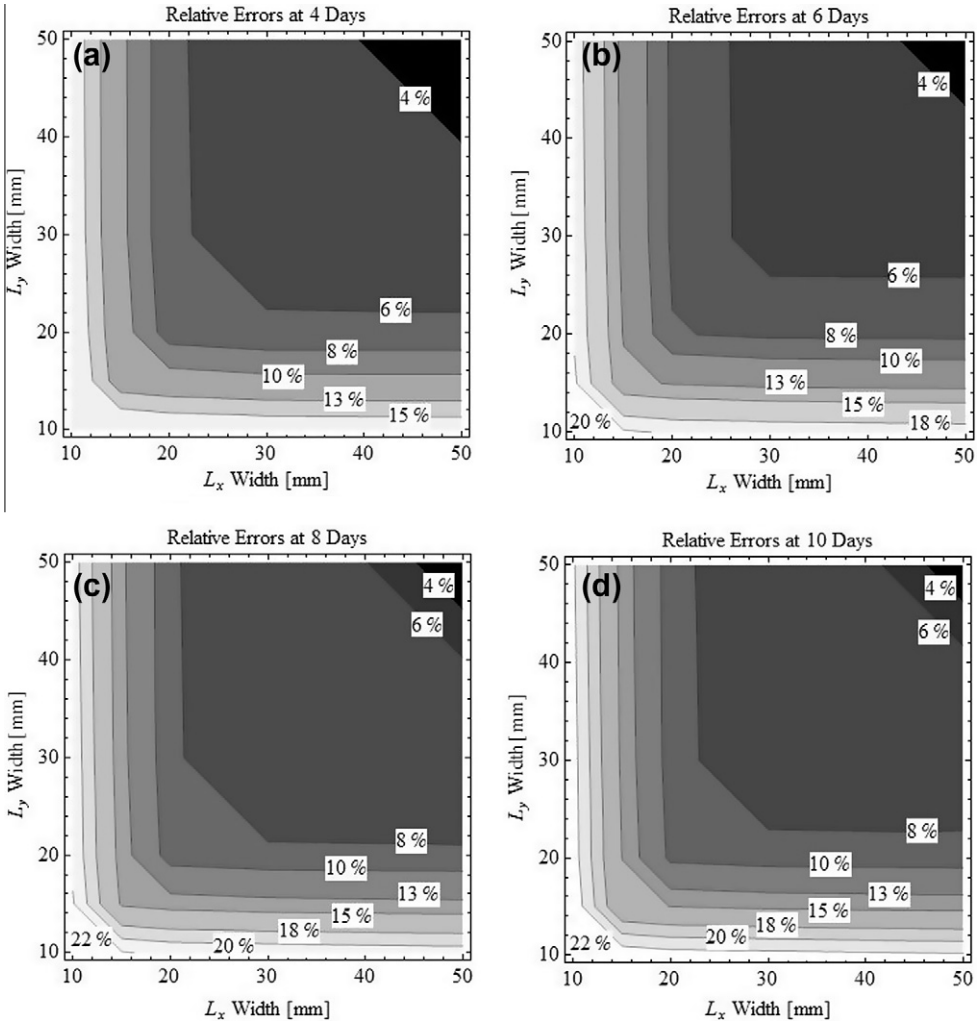

Fig. 9. Spatial error maps displaying the discrepancy in going from 3D to 1D simulations; (a) t = 4 days, (b) t = 6 days, (c) t = 8 days, (d) t = 10 days.

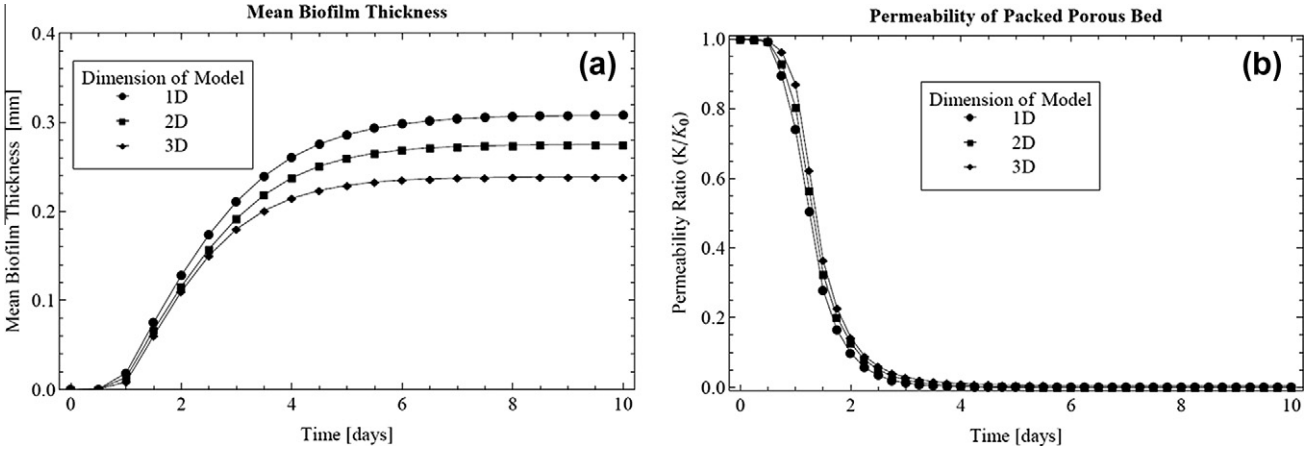

Fig. 10. Multidimensional effects of 2-species model; (a) mean thickness of 2-species biofilm growth with shearing, (b) permeability reduction of a porous bed.

2D model predictions compared to the 3D model. Fig. 7 displays the error maps when both the x and y direction lengths are changed at different times.

5.3. Comparison of one dimensional and three dimensional models

Fig. 8a and b display the growth rate predictions between the 1D and 3D models. Also shown in Fig. 8a is the comparison with the results of Wanner–Gujer [1] and Shafahi–Vafai [4]. These figures show the effects of changing the size of a square domain for 3D biofilm growth, as well as their relative differences with the 1D model. Fig. 9 shows the error map when both the x and y direction lengths are changed at different times.

The error maps show that the one dimensional and three dimensional predictions begin to diverge significantly at domain widths of around 20 mm. For domain widths greater than

20 mm, the one dimensional model predictions provide relatively similar predictions as the three dimensional models.

5.4. Comparison of one, two and three dimensional models applied to the changing permeability of a packed porous bed

Using the two species biofilm model composed of bacterial species *P. aeruginosa* and EPS, the multidimensional models are applied to investigate the changing permeability of a porous medium composed of a heterogeneously packed bed of spheres [18]. Details of the porous media model, and its various geometrical attributes, are given in Shafahi–Vafai [4].

The results for the biofilm growth and permeability ratio reduction are given in Fig. 10a and b. As noted before, the three species model has a slower growth rate in higher dimensional models. This is also the case when a two species model is considered. This leads to a slightly lower rate of decrease of the permeability of the porous bed for higher dimensional models. It is established that the one dimensional porous media model is in very good agreement with its two and three dimensional analogs.

6. Conclusions

A general multidimensional, multispecies, heterogeneous continuum biofilm model was developed. Two general case studies were analyzed for multidimensional effects, the first being a 3-species system composed of heterotrophic bacteria, autotrophic bacteria and EPS, and the second being a 2-species system composed of the bacteria *P. aeruginosa* and EPS. For the 3-species system, error maps were developed giving the relative differences of the one, two and three dimensional model predictions. For the 2-species system, the biofilm model was applied to a porous media model defined by a packed bed of spheres, and the changes in permeability were predicted and analyzed. In general, the range and validity of the one dimensional models was established and was found to cover a wide range of applications.

7. Conflict of interest

There is no conflict of interest at all.

References

[1] W. Gujer, O. Wanner, A multispecies biofilm model, Biotechnol. Bioeng. XXVIII (1986).
[2] E. Alpkvist, I. Klapper, A multidimensional multispecies continuum model for heterogeneous biofilm development, Bull. Math. Biol. (2007) 765–789.
[3] J. Dockery, I. Klapper, Finger formation in biofilm layers, Soc. Ind. Appl. Math. 62 (3) (2001) 853–869.
[4] M. Shafahi, K. Vafai, Biofilm affected characteristics of porous structures, Int. J. Heat Mass Transf. 52 (3–4) (2009) 574–581.
[5] M. Shafahi, K. Vafai, Synthesis of biofilm resistance characteristics against antibiotics, Int. J. Heat Mass Transf. 53 (2010) 2943–2950.
[6] C. Picioreanu, J.-U. Kreft, M.C.M. van Loosdrecht, Particle-based multidimensional multispecies biofilm model, Appl. Environ. Microbiol. 70 (5) (2004) 3024–3040.
[7] J.-U. Kreft, C. Picioreanu, J.W. Wimpenny, M.C. van Loosdrecht, Individual-based modeling of biofilms, Microbiology 147 (11) (2001) 2897–2912.
[8] J.U. Kreft, J.W. Wimpenny, Effect of EPS on biofilm structure and function as revealed by an individual-based model of biofilm growth, Water Sci. Technol. 43 (6) (2001) 135–141.
[9] S.W. Hermanowicz, A simple 2D biofilm model yields a variety of morphological features, Math. Biosci. 169 (1) (2001) 1–14.
[10] J.W. Wimpenny, R. Colasanti, A unifying hypothesis for the structure of microbial biofilms based on cellular automaton models, FEMS Microbiol. Ecol. 22 (1) (1997) 1–16.
[11] C. Picioreanu, M.C. van Loosdrecht, J.J. Heijnen, Mathematical modeling of biofilm structure with a hybrid differential–discrete cellular automaton approach, Biotechnol. Bioeng. 58 (1) (2000) 101–116.
[12] E. Alpkvist, C. Picioreanu, M.C. van Loosdrecht, A. Heyden, Three-dimensional biofilm model with individual cells and continuum EPS matrix, Biotechnol. Bioeng. 94 (5) (2006).
[13] B.E. Rittmann, P.L. McCarty, Model of steady-state-biofilm kinetics, Biotechnol. Bioeng. XXII (1980) 2343–2357.
[14] B.E. Rittmann, J.A. Manem, Development and experimental evaluation of a steady-state, multispecies biofilm model, Biotechnol. Bioeng. 39 (9) (1991).
[15] C. Picioreanu, M.C. van Loosdrecht, J.J. Heijnen, Discrete-differential modelling of biofilm-structure, Water Sci. Technol. 39 (7) (1999) 115–122.
[16] J.A. Sethian, Level Set Methods and Fast Marching Methods, Cambridge University Press, Cambridge, 1999.
[17] O. Wanner, A.B. Cunningham, R. Lundman, Modeling biofilm accumulation and mass transport in a porous medium under high substrate loading, Biotechnol. Bioeng. 47 (6) (1995) 703–712.
[18] S.W. Taylor, P. Milly, P.R. Jaffe, Biofilm growth and the related changes in the physical properties of a porous medium 2. Permeability, Water Resour. Res. 26 (9) (1990) 2161–2169.